

RESEARCH ARTICLE

Open Access

Developmental fates of shark head cavities reveal mesodermal contributions to tendon progenitor cells in extraocular muscles



Shunya Kuroda^{1,2*} , Noritaka Adachi³ , Rie Kusakabe¹  and Shigeru Kuratani^{1,4} 

Abstract

Vertebrate extraocular muscles (EOMs) function in eye movements. The EOMs of modern jawed vertebrates consist primarily of four recti and two oblique muscles innervated by three cranial nerves. The developmental mechanisms underlying the establishment of this complex and the evolutionarily conserved pattern of EOMs are unknown. Chondrichthyan early embryos develop three pairs of overt epithelial coeloms called head cavities (HCs) in the head mesoderm, and each HC is believed to differentiate into a discrete subset of EOMs. However, no direct evidence of these cell fates has been provided due to the technical difficulty of lineage tracing experiments in chondrichthyans. Here, we set up an *in ovo* manipulation system for embryos of the cloudy catshark *Scyliorhinus torazame* and labeled the epithelial cells of each HC with lipophilic fluorescent dyes. This experimental system allowed us to trace the cell lineage of EOMs with the highest degree of detail and reproducibility to date. We confirmed that the HCs are indeed primordia of EOMs but showed that the morphological pattern of shark EOMs is not solely dependent on the early pattern of the head mesoderm, which transiently appears as tripartite HCs along the simple anteroposterior axis. Moreover, we found that one of the HCs gives rise to tendon progenitor cells of the EOMs, which is an exceptional condition in our previous understanding of head muscles; the tendons associated with head muscles have generally been supposed to be derived from cranial neural crest (CNC) cells, another source of vertebrate head mesenchyme. Based on interspecies comparisons, the developmental environment is suggested to be significantly different between the two ends of the rectus muscles, and this difference is suggested to be evolutionarily conserved in jawed vertebrates. We propose that the mesenchymal interface (head mesoderm vs CNC) in the environment of developing EOM is required to determine the processes of the proximodistal axis of rectus components of EOMs.

Keywords: Head muscles, Head cavity, Head mesoderm, Extraocular muscles, Tendon

Background

The extraocular muscles (EOMs) connect the surface of the eye and cranial wall and function in eyeball movements. They consist primarily of four recti and two

oblique muscles and are innervated by three cranial motor nerves: the oculomotor, trochlear, and abducens nerves (Fig. 1a). The primordia of EOMs in amniotes emerge from the unsegmented head paraxial mesoderm, in contrast to segmented trunk somites [2, 3]. Moreover, nonmuscular tissues surrounding the primordia of EOMs in the so-called orbital region consist mainly of mesenchymal cells derived from cranial neural crest (CNC) cells [4]. The CNC cells in this region do not have segmental identity, as is seen in the pharyngeal

* Correspondence: shunya.kuroda@riken.jp

¹Laboratory for Evolutionary Morphology, RIKEN Center for Biosystems Dynamics Research (BDR), 2-2-3 Minatogijima-minami, Chuo-ku, Kobe 650-0047, Japan

²Department of Biology, Graduate School of Science, Kobe University, Kobe 657-8501, Japan

Full list of author information is available at the end of the article



© The Author(s). 2021 **Open Access** This article is licensed under a Creative Commons Attribution 4.0 International License, which permits use, sharing, adaptation, distribution and reproduction in any medium or format, as long as you give appropriate credit to the original author(s) and the source, provide a link to the Creative Commons licence, and indicate if changes were made. The images or other third party material in this article are included in the article's Creative Commons licence, unless indicated otherwise in a credit line to the material. If material is not included in the article's Creative Commons licence and your intended use is not permitted by statutory regulation or exceeds the permitted use, you will need to obtain permission directly from the copyright holder. To view a copy of this licence, visit <http://creativecommons.org/licenses/by/4.0/>. The Creative Commons Public Domain Dedication waiver (<http://creativecommons.org/publicdomain/zero/1.0/>) applies to the data made available in this article, unless otherwise stated in a credit line to the data.

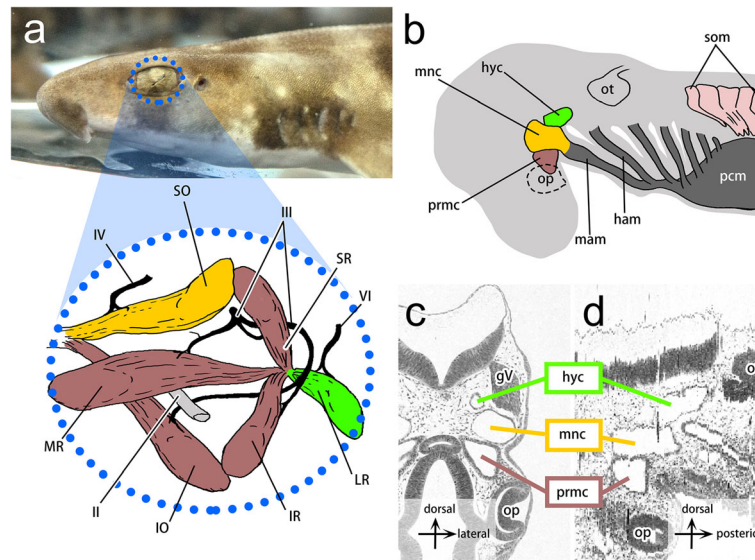


Fig. 1 Anatomy of EOMs and distributions of head cavities in the shark embryo. **a** Left lateral view of an adult shark (*S. torazame*; top) and schematic drawing of the left extraocular muscles (bottom). Sets of EOMs innervated by the same cranial motor nerve are shown in the same color: EOMs innervated by the oculomotor nerve in brown, by the trochlear nerve in orange, and by the abducens nerve in green. The blue dotted line indicates the outline of the left eye. **b** A schematic drawing of the left lateral view of the shark embryo at st. 25 showing the positional relationships of head cavities (HCs) to the pharyngeal and cardiac mesoderm (dark gray) and somites (light pink). Each HC is marked in the same color as sets of EOMs in **(a)**, which are predicted to be derived from a single HC. **c, d** H&E sections in the transverse section **(c)** and the sagittal section reconstructed from serial transverse sections **(d)**, showing the anatomical position of HCs, which are arranged in series dorsoventrally **(c)** and anteroposteriorly **(d)**. The scheme in **(a)** is modified from ref. [1]. II, optic nerve; III, oculomotor nerve; IV, trochlear nerve; VI, abducens nerve; gv, trigeminal ganglion; ham, hyoid arch mesoderm; IO, inferior oblique muscle; IR, inferior rectus muscle; LR, lateral rectus muscle; mam, mandibular arch mesoderm; mnc, mandibular head cavity; MR, medial rectus muscle; op, optic cup; ot, otic vesicle; pcm, pericardial mesoderm; prmc, premandibular head cavity; SO, superior oblique muscle; som, somite; SR, superior rectus muscle

arches, since they are located anterior to the first pharyngeal arch [5–7].

The mesenchymal state of the head mesoderm is commonly seen in most experimental animals throughout development [8, 9]. In contrast, embryos of chondrichthyans (cartilaginous fishes) generally form three pairs of epithelial coeloms called head cavities (HCs) (Fig. 1b–d) [1, 10–13]. The premandibular head cavity (prmc) originates from the prechordal plate, the anteriormost element of the axial mesoderm, that is, from the anteriormost mesoderm in the vertebrate embryo. The mandibular head cavity (mnc) and hyoid head cavity (hyc), on the other hand, are derived from the head paraxial mesoderm (Fig. 1b–d) [12]. Both HCs arise as schizocoels between the neurula and early pharyngula stages [12]. In later stages, histological observations have shown that the epithelial walls of HCs collapse and that the coelomic structures gradually disappear [14]. Each of the HCs was assumed to give rise to a distinct subset of EOMs innervated by a single cranial nerve (Fig. 1a). Therefore, the morphology of HCs has long been believed to serve as a prepattern for EOM morphology [11, 15–17]. However, this predicted lineage of HCs has only

been roughly illustrated by histological observations of developmental series of elasmobranch embryos (sharks, skates, and rays) [10, 14]. To elucidate the detailed cell fates of each HC, cell lineage tracing experiments are required. Moreover, the developmental contributions of HCs to nonmuscular tissues also remain to be investigated [11, 12, 18–20].

In the present study, we examined the developmental fates of shark HCs to determine whether each of the HCs gives rise to a different set of EOMs or other musculoskeletal components. The epithelial nature of shark HCs facilitates accurate and highly reproducible labeling of a specific part of the head mesoderm, which in other animals appears only as a cluster of mesenchymal cells without discrete histological boundaries [9, 21, 22]. We performed lineage tracing experiments using a lipophilic fluorescent dye in embryos of the cloudy catshark *Scyliorhinus torazame* (Tanaka, 1908) [23], which has three pairs of HCs [5, 12]. We confirmed that the HCs give rise to EOMs but also discovered that the cell fates of HCs were more complex than classically predicted (Fig. 1). We further revealed that HCs also give rise to tendon progenitor cells for some of the rectus muscles.

Methods

Embryo collection

Fertilized eggs of *S. torazame* were collected from tanks of adult sharks kept at 16 °C at RIKEN. Embryos were staged according to a previous study [24]. For section in situ hybridization and immunohistochemistry, embryos were fixed overnight in 4% paraformaldehyde (PFA) (104,005; Merck KGaA, Germany) in phosphate-buffered saline (PBS) (pH 7.4, AM9625; Thermo Fisher Scientific, USA) at 4 °C.

Molecular cloning and phylogenetic analysis

Total RNA of *S. torazame* was extracted using TRIzol Reagent (15,596,026; Thermo Fisher Scientific), and the corresponding cDNA was synthesized using SuperScript IV Reverse Transcriptase (18,091,050; Thermo Fisher Scientific). PCR was performed to amplify fragments of the *S. torazame Scleraxis (StScx)* gene by LA Taq HS (RR042A; TaKaRa Bio Inc., Japan) with specific primers designed based on the prospective *StScx* sequence obtained from Squalomix, the elasmobranch transcriptome database (<https://transcriptome.riken.jp/squalomix/>) [25]. The PCR fragments were cloned into the pGEM-T Easy vector (A1360; Promega, USA) and sequenced. For phylogenetic analysis, amino acid sequences of orthologous genes from other vertebrate and invertebrate species were compiled from GenBank (<http://www.ncbi.nlm.nih.gov/>) and Ensembl (<http://www.ensembl.org/>). Multiple alignments of protein sequences were performed with MAFFT [26] as implemented on the web server of the European Bioinformatics Institute (<http://www.ebi.ac.uk/Tools/msa/mafft/>) and saved in FASTA format. The resulting alignments were trimmed by trimAl version 1.3 as implemented in Phylemon 2.0 [27] and aligned using ClustalW (<http://www.clustal.org/>) without gaps. Phylogenetic trees were constructed using the maximum-likelihood (ML) method in PhyML v.3.1 (<http://www.atgc-montpellier.fr/phyml/>) [28] to confirm the orthology of the *StScx* gene (Fig. S1).

Fate mapping and embryonic culture in sharks

For the injection of shark embryos at stage 25, eggs were removed from the seawater tank and briefly incubated on ice. A small window was opened on the surface of the egg case just above the embryo. Embryos were then anesthetized with 20 µl of a mixed solution of 1% ethyl 3-aminobenzoate methanesulfonate (MS-222) (E10521; Sigma) and 2% sodium carbonate (1:1 volume:volume). CM-DiI (C7001; Thermo Fisher Scientific, USA) was prepared as previously described [29] and microinjected into HCs by using a microinjector (MN-151; Narishige, Japan). After injection, 200 µl of 0.2% antibiotic-antimycotic mixed stock solution (09366-44; Nacalai Tesque, Inc., Japan) in PBS was added to the surface of

the embryo. The eggshell was sealed with a polycarbonate filter (GTBP01300; Merck Millipore, USA) using cyanoacrylate adhesive (Aron Alpha, also known as 'Krazy Glue'; Toagosei, Japan), to prevent air bubbles from entering the eggshell and to prevent the contents of the egg from protruding through the opening. The injected embryos were left to develop for 6–7 weeks at 16 °C in seawater with 0.2% antibiotic-antimycotic mixed stock solution without aeration. The incubation seawater was replaced multiple times weekly.

Histological analysis and in situ hybridization

Fixed embryos were dehydrated and embedded in paraffin (Paraplast Plus, P3683; Sigma-Aldrich) at 65 °C. Sections were cut at a thickness of 7 µm. For fluorescence detection of CM-DiI-labeled samples, the deparaffinized sections were washed twice with PBS and incubated for 1 h at room temperature with 4',6-diamidino-2'-phenylindole dihydrochloride (DAPI) (5 µg/ml, 10,236,276,001; Roche, Switzerland) in PBS. Then, drops of Omnipaque300 (Daiichi-Sankyo, Japan) were added to the sections, and the coverslips were placed. The sections were then imaged by using an Axio Zoom V16 fluorescence microscope (Carl Zeiss, Germany) with an AxioCam MRm digital camera (Carl Zeiss). For immunostaining, the sections were washed with Tris-HCl-buffered saline (pH 7.8, 20 mM Tris-HCl, 150 mM NaCl) containing 1% Triton X-100 (TST), blocked with 5% skim milk in TST (TSTM) for 30 min, and incubated overnight at room temperature with primary antibodies diluted in TSTM. Myosin heavy chain antibody (1/200, A4-1025; DSHB) was used as a primary antibody. After 3 washes in TST (5 min each), the sections were incubated with secondary antibodies in TSTM for 2 h at room temperature. Anti-mouse IgG horseradish peroxidase (HRP) antibody (1/400, F21453; Thermo Fisher Scientific, USA) was used as a secondary antibody. HRP activity was detected using 0.25 mg/ml peroxidase substrate, 3,3'-diaminobenzidine (DAB) (D5905-50TAB; Sigma), in TST with 0.01% hydrogen peroxide. Hematoxylin and eosin (H&E) or Alcian blue staining was performed according to a standard protocol. The sagittal section in Fig. 1d was reconstructed in silico from serial transverse sections using Avizo software version 8.0.1 (Thermo Fisher Scientific). In situ hybridization on paraffin sections for *S. torazame Scx* (GenBank accession number LC430615) was performed as previously described [30]. Counterstaining for in situ hybridization was performed with Nuclear Fast Red (Vector Laboratories, USA). Adjacent sections were analyzed to compare gene expression patterns and distributions of fluorescently labeled cells. Sections in brightfield images were imaged with

a BX53 microscope (Olympus, Japan) with a DP74 digital camera (Olympus). Fluorescent images were processed by ZEN software (Carl Zeiss), and all images were assembled in Adobe Photoshop (Adobe Systems, USA) as previously described [31].

Results

Long-term cell lineage tracing in *S. torazame* embryos

In stage 25 (st. 25) *S. torazame* embryos, three pairs of HCs were fully formed but had not yet begun their differentiation into muscle cells (Fig. 1b-d) [12, 14]. We attempted to label the epithelial wall of each HC by microinjecting CM-DiI into the coelom (Fig. 2a, c, and e). Since the left and right sides of the prmc at this stage are connected through a transverse canal just behind Rathke's pouch [10, 12], when DiI was injected into one side of the prmc, the opposite side of the prmc was also labeled at a certain frequency (7 cases in 12 injected embryos). In contrast, the left and right coeloms of the mnc and hyc were separated from each other (Fig. 1b-d), and we could label each of the HCs specifically with our

method. We fixed embryos at 12 hours postinjection (0.5 dpi) and confirmed that CM-DiI labeling was confined to the epithelial wall of the injected coelom (number of times that DiI was specifically recovered in labeled embryos: prmc, $n = 3/4$; hyc, $n = 5/7$; mnc, $n = 3/5$) (Fig. 2). Although the ventral portion of the mnc connected with the tubular pharyngeal arch mesoderm (Fig. 1b), the lumen of the pharyngeal arch canal was almost flattened and very narrowed by this stage [12], preventing ectopic dye labeling outside the mnc. Moreover, no DiI-labeled cells were observed in other tissues around HCs, ensuring exclusive labeling of the HC epithelium (Fig. 2b', d', and f').

In the following experiments, we incubated DiI-injected embryos until st. 31 (42 dpi; Fig. 3a), by which time all EOMs were differentiated and connected to their attachment sites.

We used myosin heavy chain (MyHC) antibody and Alcian blue staining to identify muscles and skeletal tissues in the developed embryos. To visualize tendon progenitor cells, we isolated a shark homologue of the

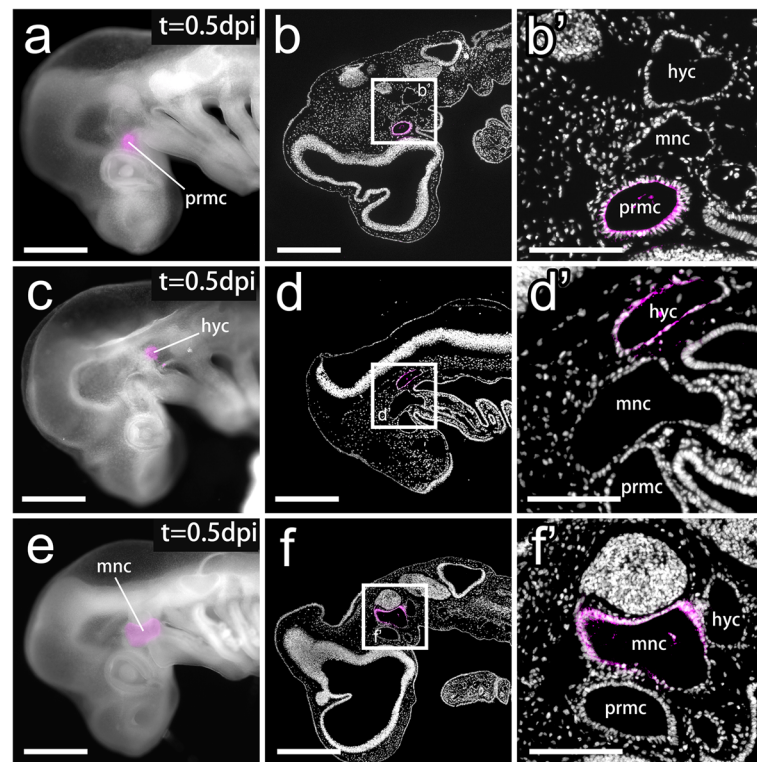


Fig. 2 DiI-labeled head cavities at the pharyngula stage. **a-b'** An embryo with DiI injected into the prmc at st. 25. **a** Left lateral view of the DiI-injected embryo at 0.5 days postinjection (dpi). **b-b'** A sagittal section of **(a)** and a magnified image in the inset **(b')** showing DiI-labeled cells (magenta) found specifically in the epithelial wall of the prmc. **c-d'** An embryo with DiI injection into the hyc at st. 25. **c** Left lateral view of the DiI-injected embryo at 0.5 dpi. **d-d'** A sagittal section of **(c)** and a magnified image in the inset **(d')** show DiI-labeled cells (magenta) found specifically in the epithelial wall of the hyc. **e-f'** An embryo with DiI injection into the mnc at st. 25. **e** Left lateral view of a DiI-injected embryo at 0.5 dpi. **f-f'** A sagittal section of **(e)** and a magnified image in the inset **(f')** show DiI-labeled cells (magenta) found specifically in the epithelial wall of the mnc. Panels **b, b', d, d', f, and f'** show sections counterstained with DAPI (gray). hyc, hyoid head cavity; mnc, mandibular head cavity; prmc, premandibular head cavity. Scale bars = 500 μ m (**a, b, c, d, e, and f**), 200 μ m (**b', d', and f'**)

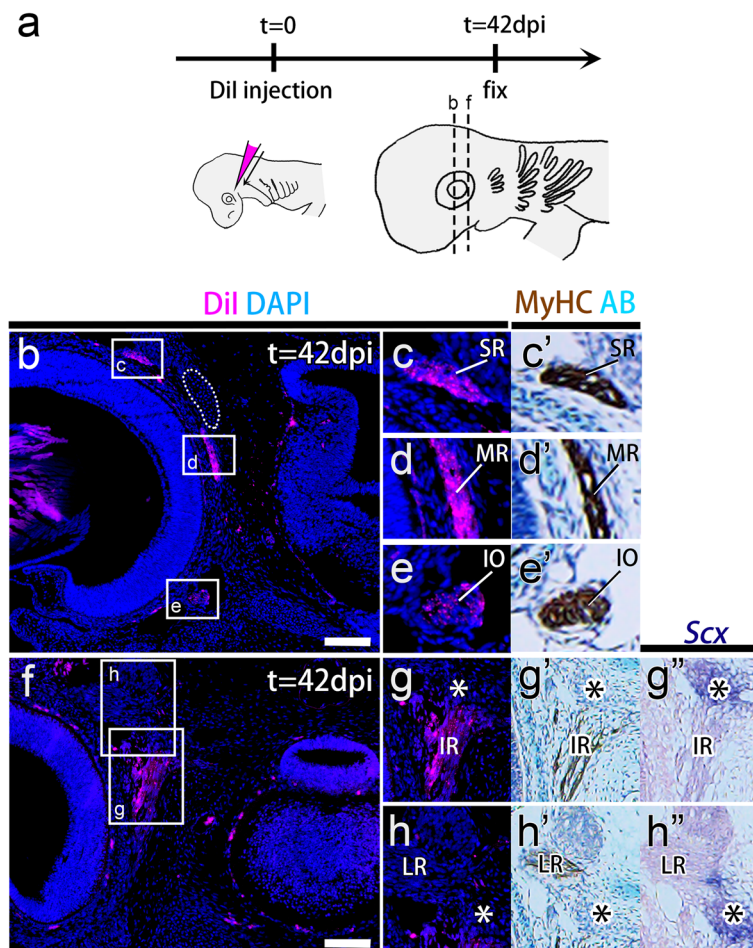
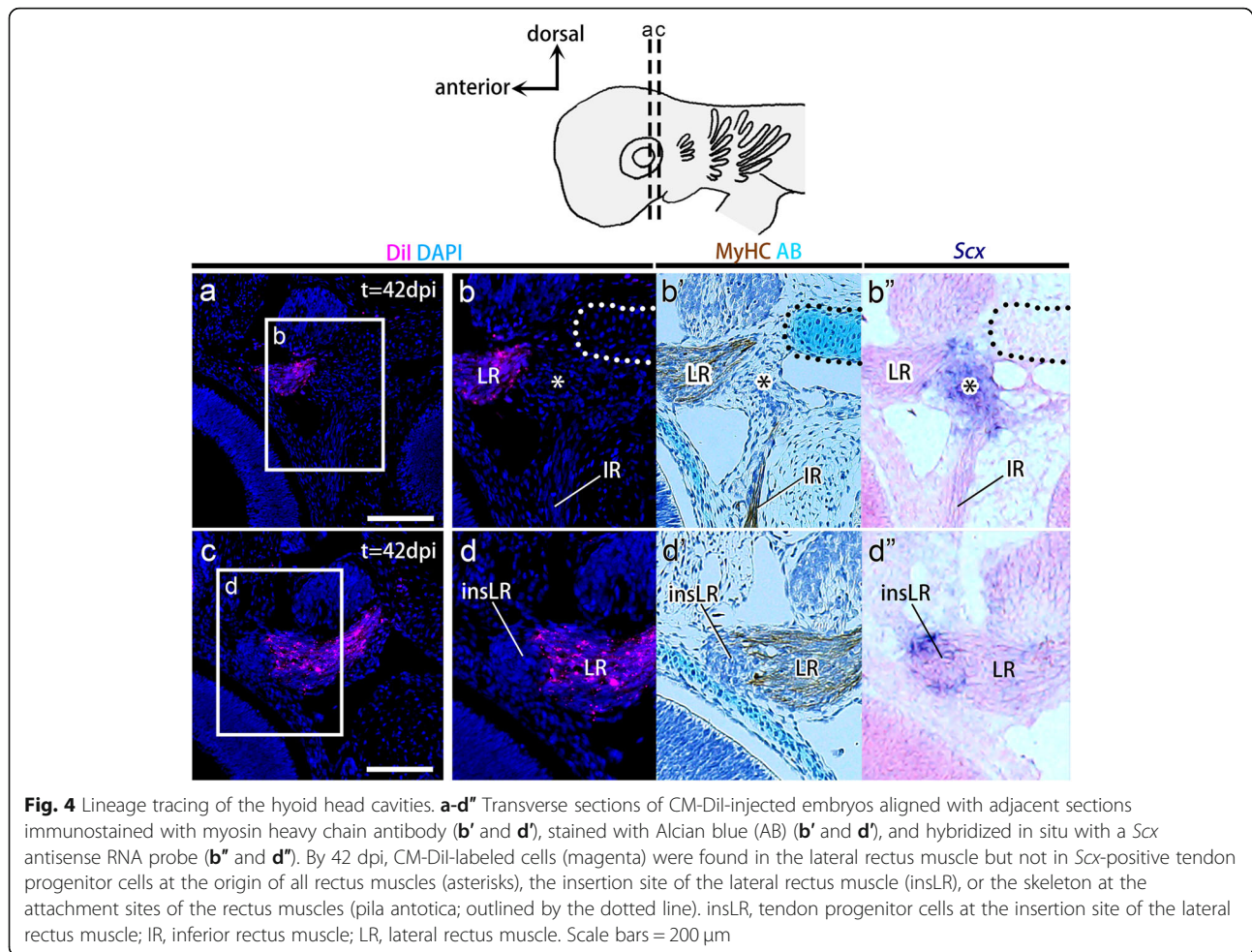


Fig. 3 Lineage tracing of the premandibular head cavities. **a** Dil was injected into the coelom of the prmc of a cat shark embryo at st. 25. At st. 31 (42 days postinjection: 42 dpi), the Dil-injected embryos were fixed and histologically examined. **b-h** Transverse sections cut through the dashed lines in **(a)** Dil-injected catshark embryos at 42 dpi. Sections **(b)** and **(f)** were each aligned with adjacent sections immunostained with anti-myosin heavy chain (MyHC) antibody **(c', d', e', g', and h')**, stained with Alcian blue (AB) **(c', d', e', g', and h')**, and hybridized in situ with a *Scx* antisense RNA probe **(g'' and h'')**. Dil-labeled cells (magenta) are found in muscle fibers of specific sets of extraocular muscles (superior rectus, medial rectus, inferior oblique, and inferior rectus muscles) but not in *Scx*-positive tendon progenitor cells at the attachment site of all rectus eye muscles (asterisks) or in the pila antotica (outlined by the dotted line). IO, inferior oblique muscle; IR, inferior rectus muscle; LR, lateral rectus muscle; MR, medial rectus muscle; SR, superior rectus muscle. Scale bars = 200 μ m

Scleraxis (*Scx*) gene, which is known to be expressed in tendon progenitor cells in mice [32], chickens [33], and zebrafish [34]. In situ hybridization analysis confirmed that *S. torazame Scx* expression was specifically detected in cell condensations, which are presumptive tendon progenitor cells, located between the jaw muscle and cartilage (Fig. S2b). Using this *Scx* probe, MyHC antibody and Alcian blue as tissue-specific markers for tendon progenitor cells, differentiated muscles and cartilage, respectively, we examined the distribution of Dil-labeled cells derived from each HC in the established musculoskeletal components, as described below.

The premandibular and hyoid head cavities give rise to distinct sets of EOMs

In the embryos injected with Dil into the prmc, labeled cells were observed in muscle fibers of the superior rectus ($n = 17/19$) (Fig. 3c), medial rectus ($n = 18/19$) (Fig. 3d), inferior oblique ($n = 14/19$) (Fig. 3e), and inferior rectus muscles ($n = 19/19$) (Fig. 3g) stained by anti-MyHC antibody (Fig. 3b-h'). Dil-labeled cells were not detected in Rathke's pouch ($n = 0/12$) (Fig. S3a), the trigeminal ganglia ($n = 0/19$) (Fig. S3b), optic vesicles ($n = 0/19$) (Fig. S3c), sclera ($n = 0/19$) (Fig. S3c), the chondrocranium at the attachment sites of rectus muscles (pila antotica [35, 36];) ($n = 0/19$) (Fig. 3b), or the trabecular



cartilage ($n = 0/19$) (Fig. S3d). At the same time, DiI-labeled cells rarely emerged in polar cartilage ($n = 1/19$) (Fig. S3d) and tendon progenitor cells at the origin of the rectus muscles ($n = 7/19$) (Fig. 3g-h''). In the embryos injected with CM-Dil into the hyc, labeled cells were recovered in the lateral rectus muscle fibers ($n = 15/15$) (Fig. 4b, b', d, and d'). Labeling was undetectable in the trigeminal ganglia ($n = 0/15$) (Fig. S4) and was only rarely detected in the pila antotica ($n = 1/15$) (Figs. 4b-b'', and S4) and two tendon progenitor elements (at the origin of rectus muscles; $n = 7/15$ and at the insertion of lateral rectus muscle; $n = 8/15$) (Fig. 4).

These findings demonstrate that prmc and hyc give rise to the oculomotor nerve- and abducens nerve-innervated components of EOMs, respectively (Fig. 1a), which is in line with previous histological observations (Fig. 1) [17, 37]. Moreover, neither the prmc nor the hyc was suggested to give rise to cartilage or tendon.

The mandibular head cavity gives rise to tendon progenitor cells as well as muscle fibers

The labeling of the mnc provided both expected and unexpected results. DiI-labeled cells were recovered in the superior oblique muscle fibers ($n = 19/22$) that were positive for MyHC (Fig. 5a-b'), suggesting that the mnc gives rise to the trochlear nerve-innervated EOM (Fig. 1a). DiI-labeled cells were also detected at the point of origin of all rectus muscles (asterisks in Fig. 5d-d') and at the insertion site of the lateral rectus muscle (insLR in Fig. 5f-f') at high frequencies ($n = 16/22$ and $n = 22/22$, respectively). These attachment sites were marked by *Scx* expression (Fig. 5d'' and f''), showing the features of tendon progenitor cells (see also Fig. S2). No labeled cells were found in other tendon progenitors ($n = 0/22$) (Fig. 5), the pila antotica ($n = 0/22$) (Fig. 5d-d''), orbital cartilage ($n = 0/22$) (Fig. S5a), trabecular cartilage ($n = 0/22$) (Fig. S5b), or palatoquadrate cartilage ($n = 0/22$) (Fig. S5d). These results provide the first evidence that the epithelial wall

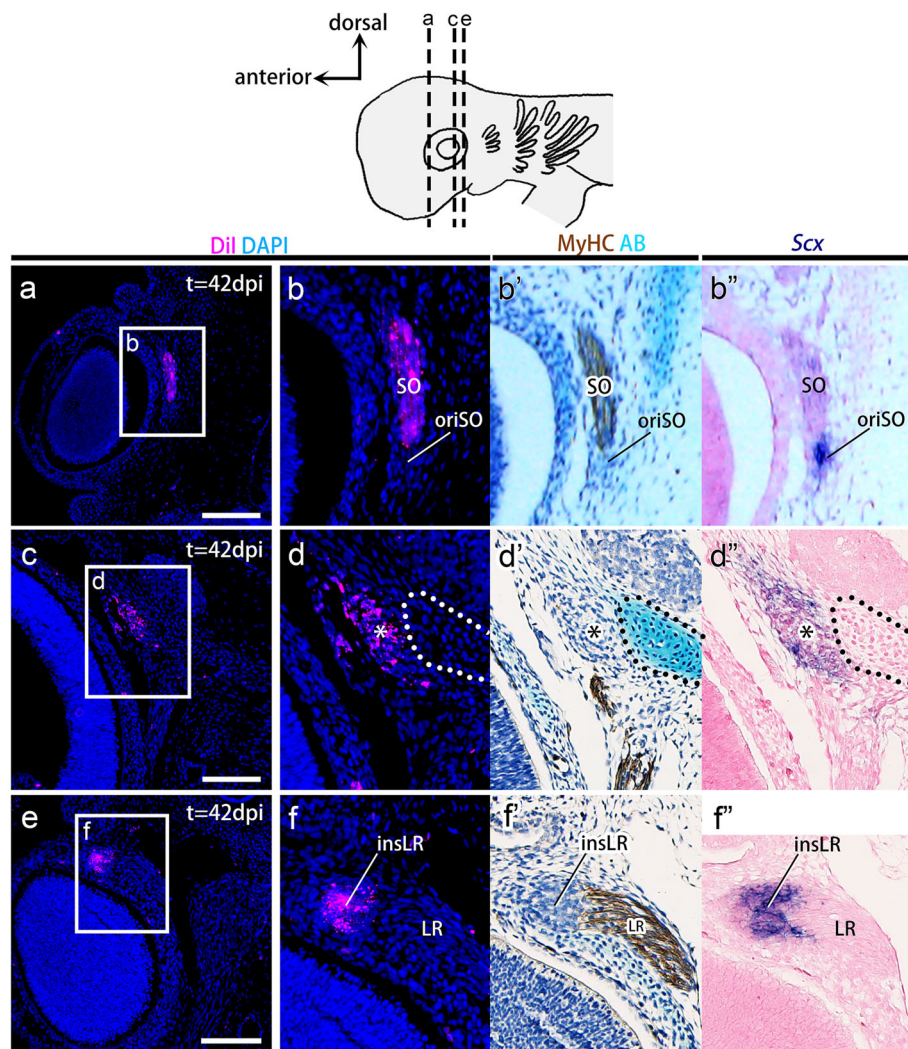


Fig. 5 Lineage tracing of the mandibular head cavities. **a-f''** Transverse sections of CM-Dil-injected embryos aligned with adjacent sections immunostained with myosin heavy chain antibody (**b'**, **d'**, and **f'**), stained with Alcian blue (AB) (**b'**, **d'**, and **f'**), or hybridized in situ with an *Scx* antisense probe (**b''**, **d''**, and **f''**). By 42 dpi, Dil-labeled cells (magenta) were found in the superior oblique muscle, and the *Scx*-positive tendon progenitor cells were found at the scaffold of all rectus eye muscles (asterisks) and the insertion site of the lateral rectus muscle (*insLR*). *insLR*, tendon progenitor cells at the insertion site of the lateral rectus muscle; LR, lateral rectus muscle; SO, superior oblique muscle. Scale bars = 200 μ m

of the *mnc* in shark embryos, as a part of the head mesoderm, gives rise to specific tendon progenitor cells in addition to trochlear nerve-innervated EOMs (superior oblique muscle; Fig. 1d) [17, 37].

Discussion

In this study, we reported lineage tracing analysis of HCs in shark embryos and showed that each HC gives rise to a set of EOMs innervated by a single cranial motor nerve (Figs. 1d and 6). In addition, our results provide the first evidence that HCs, which belong to the head mesoderm, give rise to dense connective tissues of the head muscles in shark; the *mnc* gives rise to tendon

progenitor cells at the origin of the rectus muscles and at the insertion of lateral rectus muscles (Fig. 6d and e). In contrast, we did not observe any contributions from HCs to the cranial cartilage in our experiments.

Concerning the *mnc*-derived cellular condensation at the insertion site of the lateral rectus muscle, given its position and developmental origin, it could be the same cell population first described by Platt as 'muscle E' (Fig. S6, [14, 15, 38, 39]). Platt and later researchers thought that this condensation gives rise to muscle cells of the distal portion of the lateral rectus muscle (reviewed in [15]). However, in our experiments, this condensation was not positive

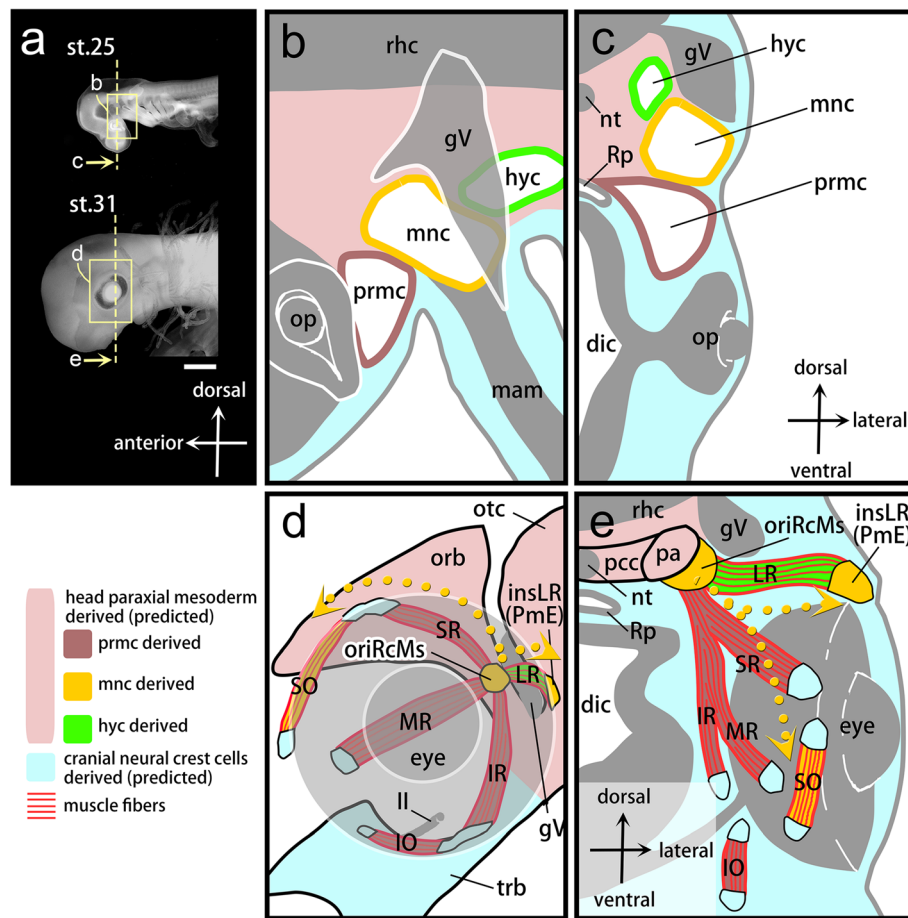


Fig. 6 Developmental fates of shark head cavities in the musculoskeletal system of extraocular muscles. **a** Left lateral view of the shark embryos at st. 25 (top) and st. 31 (bottom). **b, c** Schematic drawings of a left lateral view of the inset in **(a)** and a transverse section at the level of the dashed line in **(a)** showing HCs arranged along the anteroposterior axis **(b)** and the dorsoventral axis **(c)** in the embryonic head at st. 25. **d, e** Schematic drawings of a left lateral view of the inset in **(a)** and a transverse section at the dashed line level in **(a)** showing musculoskeletal connections in EOMs via tendons at st.31. The colors of each musculoskeletal component correspond to its developmental origin, shown in **(b)** and **(c)**. Yellow dotted arrows represent the dynamic migratory pathways of mnc-derived cells reconstructed based on the results of the present study. The developmental fate of CNC cell-derived tendons (light blue) and mesodermal chondrocranium (pink) are based on the prediction. II, optic nerve; dic, diencephalon; gv, trigeminal ganglion; hyc, hyoid head cavity; insLR, a tendon at the insertion of the lateral rectus muscle; IO, inferior oblique muscle; IR, inferior rectus muscle; LR, lateral rectus muscle; mam, mandibular arch mesoderm; mnc, mandibular head cavity; MR, medial rectus muscle; nt, notochord; op, optic cup; orb, orbital cartilage; oriRcMs, a tendon at the origin of four-rectus muscles; otc, otic capsule; pa, pila antotica; pcc, parachordal cartilage; pm, PmE, Platt's 'muscle E'; prmc, premandibular head cavity; rhc, rhombencephalon; Rp, Rathke's pouch; SO, superior oblique muscle; SR, superior rectus muscle; trb, trabecular cartilage. Scale bars = 1 mm. Not to scale **(b-e)**.

for the MyHC antibody but did express the *Scx* gene, suggesting that these cells are tendon progenitor cells (Figs. 5 and S6b).

Although the classical studies that predicted the developmental fate of HCs (Fig. 1) were partially supported by our experiments, the actual developmental patterns and processes of the mnc-derived cells turned out to be more complex than was predicted (Fig. 6). Classical studies regarded the pattern of HCs as a prepattern of EOM morphology based on the predicted one-to-one correspondence between an HC and the innervation patterns of EOMs [1, 11, 15, 17]. The results of the present study led us to revise the above hypothesis. One portion

of mnc-derived cells retain their original positions throughout development and give rise to tendon progenitor cells at the origin of rectus muscles (Fig. 6). In contrast, the remaining mnc-derived cells show two different migratory pathways, one toward the anterior portion and the other toward the posterior portion of the eye (yellow dotted arrows in Fig. 6d and e). First, the superior oblique muscle primordium, separated from the dorsal part of the mnc, passes above the eye and overtakes the cell population derived from the prmc. At this point, the original anteroposterior arrangement of the HCs was altered. In the posterior part of the eye, the mnc-derived cells give rise to tendon progenitor cells at

the insertion of the lateral rectus muscle (Platt's 'muscle E'), keeping their leading position relative to the direction of movement of the lateral rectus muscle primordium. It is worth noting here that *mnc*-derived tendons are not recruited in the muscle attachment of the superior oblique muscles. This may be comparable to the relationship between the syndetome and migratory muscle precursors, both of which are derived from a single somite [40, 41]. However, because the *mnc*-derived tendons give scaffolds at both ends of the *hyc*-derived lateral rectus muscles (Fig. 6), it is still unreasonable to compare the relationship between the *mnc* and *hyc* with that of two adjacent somites. Overall, we conclude that the morphological pattern of HCs is not a prepattern of EOMs.

Reevaluating the mesoderm/CNC boundary in the mesenchymal environment in the orbital region

The majority of the mesenchymal component in the vertebrate embryonic head is derived from CNC cells [4, 42]. Since CNC cells differentiate into the pharyngeal skeleton, prechordal cranium, and connective tissues of the head muscles, it has been presumed that musculo-skeletal connections in the head would be established through interactions between CNC cells and muscle progenitor cells [4, 42–45]. In heterotopic transplantation of the trunk paraxial mesoderm into the head, grafted cells gave rise to head muscles with nearly normal morphology [46, 47]. In *Tbx1* knockout mice, branchiomeric muscle precursors were absent, but the initial patterning of tendon progenitor cells occurred normally [48]. Thus, the morphogenetic information of the CNC cells that give rise to dense connective tissues in the head can override the identity of the muscle precursors exposed in the ectomesenchymal environment (derived from CNC cells) [49–52].

EOM primordia first appear in the head paraxial mesoderm, where they are detectable by *Pitx2* expression, and subsequently migrate rostrally to enter ectomesenchymal environments in the prechordal region [50, 53, 54]. This migration pattern led to the belief that CNC cells would be the only origin of the dense connective tissues of EOMs, as in the case of other head muscles [4, 42]. CNC cells were confirmed to contribute to some part of the connective tissues of EOMs using chick/quail chimeric embryos [51] and transgenic mice [55]. On the other hand, the skeletal component at the proximal attachment sites (origins) of four rectus components of EOMs is known to be mesodermal in mice and chickens [43, 56]. The latter results suggest that the developing rectus muscles may be on the mesenchymal interface between the head paraxial mesoderm and CNC cells. In the present study, we revealed the contributions of the head mesoderm to tendon progenitor

cells at the proximal attachment of rectus muscles in sharks. This result is consistent with the above discussion about the position of the mesoderm/CNC interface in the orbital region. At the same time, this suggests that the corresponding EOM attachment sites in mice (*ala hypochiasmatica*) and chickens (supratrabecular cartilage) also adopt mesodermal tendons similar to those in shark embryos (Fig. S7). Now, we need to reexamine the cell lineages of connective tissues of EOMs in these two animals, for whom the cell lineages of the structures in the head have been studied in greater detail than in any other vertebrate.

In the present study, we could not perform lineage tracing experiments of shark CNC cells due to technical difficulties. Considering the results of previous experiments in model animals that have shown that the periorcular mesenchyme generally consists of CNC cells [55, 57, 58], it is reasonable to speculate that the other tendons in shark EOMs that are not derived from HCs are derived from CNC cells (Fig. 6d and e). Thus, the rectus muscles other than the lateral rectus muscles in sharks are suggested to have CNC-derived tendons at one attachment site and mesodermal tendons at the other sites. The fact that some EOMs have tendons other than CNC-derived tendons suggests that the morphogenetic process of EOMs may be partially free from the identity imposed by the ectomesenchymal environment. Although our results did not support the notion that the morphological pattern of the HCs contributed to that of the EOMs, the cell population boundary in the mesenchymal environment in the orbital region might play some role in establishing the proximodistal axis in the rectus muscles.

Contexts similar to the developmental environment suggested in the present study have recently been reported in some neck and shoulder musculatures. These muscles develop in embryonic environments with mesenchymal boundaries between the CNC and lateral plate mesoderm [59] or cardio-pharyngeal mesoderm [60]. The resultant muscles have heterogeneous cell populations of connective tissues. Furthermore, considering the recent report of mesodermal contributions to the posterior part of the pharyngeal skeleton in skate [61] and to the tendon progenitor cells for EOMs in shark (this study), we have to reconsider the rather dualistic view that the morphogenetic processes in head and trunk musculature are regulated strictly by CNC-derived and mesodermal mesenchymal environments, respectively. Further clarification of the developmental mechanisms shared by muscles that develop at the mesoderm/CNC boundary will shed new light on the question of what factors determine the evolutionary coupling or decoupling between the mesoderm/CNC boundary and

the morphological boundary in craniofacial and neck-shoulder complexes [56, 62–64].

Conclusions

In our lineage tracing analysis in shark HCs, we confirmed the classical view of the developmental origin of EOMs; each HC gives rise to different subsets of EOMs innervated by each cranial motor nerve. We also found that the mnc gives rise to tendon progenitor cells at the origin of the rectus muscles and the insertion of the lateral rectus muscle. Given these newly revealed cell fates of shark HCs, we conclude that the previous hypothesis that the EOM developmental pattern was prespecified in HCs should be revised. Our results also suggest that the developmental origins of tendon progenitor cells at either end of most rectus muscles in sharks differ from each other. We speculate that the presence of the head mesoderm/CNC boundary in the mesenchymal environment could be required for establishing the proximodistal axis of the rectus components of EOMs.

Supplementary Information

The online version contains supplementary material available at <https://doi.org/10.1186/s40851-021-00170-2>.

Additional file 1.

Acknowledgments

We would like to thank K. Shirato for his help with shark fishing; E. Momota, K. Yamamoto and S. Shibuya for the maintenance of adult sharks; and K. Onimaru for helpful advice on the incubation of shark embryos.

Authors' contributions

S. Kuroda and S. Kuratani conceived the project and designed the experiments; S. Kuroda, N. A., and R. K. performed the experiments. All authors wrote the manuscript and approved the final version of the manuscript.

Funding

This work was supported by a Grant-in-Aid for Scientific Research on Innovative Areas (Research in a Proposed Research Area) no. 17H06385 to S. Kuratani and by a Grant-in-Aid for Scientific Research (C) no. 19K06683 to R. K.

Availability of data and materials

The newly identified cDNA sequence of the *S. torazame Scx* gene has been registered in GenBank under accession number LC430615. Any other relevant data are available from the corresponding author upon reasonable request.

Ethics approval and consent to participate

All animal experiments were carried out with the approval of the Institutional Animal Care and Use Committee of RIKEN, Kobe Branch.

Consent for publication

Not applicable.

Competing interests

The authors declare that they have no competing interests.

Author details

¹Laboratory for Evolutionary Morphology, RIKEN Center for Biosystems Dynamics Research (BDR), 2-2-3 Minatogijima-minami, Chuo-ku, Kobe 650-0047, Japan. ²Department of Biology, Graduate School of Science, Kobe

University, Kobe 657-8501, Japan. ³Aix-Marseille Université, CNRS, IBDM UMR 7288, 13288 Marseille, France. ⁴Laboratory for Evolutionary Morphology, RIKE N Cluster for Pioneering Research (CPR), 2-2-3 Minatogijima-minami, Chuo-ku, Kobe 650-0047, Japan.

Received: 13 November 2020 Accepted: 27 January 2021

Published online: 15 February 2021

References

1. Goodrich ES. Studies on the structure and development of vertebrates. London: McMillan; 1930.
2. Bothe I, Dietrich S. The molecular setup of the avian head mesoderm and its implication for craniofacial myogenesis. *Dev Dyn*. 2006;235(10):2845–60.
3. Kuratani S. Craniofacial development and the evolution of the vertebrates: the old problems on a new background. *Zool Sci*. 2005;22(1):1–19.
4. Noden DM. The embryonic origins of avian cephalic and cervical muscles and associated connective tissues. *Am J Anat*. 1983;168:257–76.
5. Kuratani S, Horigome N. Developmental morphology of branchiomeric nerves in a cat shark, *Scyliorhinus torazame*, with special reference to rhombomeres, cephalic mesoderm, and distribution patterns of cephalic crest cells. *Zool Sci*. 2000;17(7):893–910.
6. Minoux M, Rijli FM. Molecular mechanisms of cranial neural crest cell migration and patterning in craniofacial development. *Development*. 2010;137(16):2605–21.
7. Kuratani S, Adachi N, Wada N, Oisi Y, Sugahara F. Developmental and evolutionary significance of the mandibular arch and prechordal/premandibular cranium in vertebrates: revising the heterotopy scenario of gnathostome jaw evolution. *J Anat*. 2013;222(1):41–55.
8. Kuratani S, Adachi N. What are head cavities? — a history of studies on vertebrate head segmentation. *Zool Sci*. 2016;33(3):213–28.
9. Gilbert PW. The origin and development of the head cavities in the human embryo. *J Morphol*. 1952;90:149–87.
10. Wedin B. The anterior mesoblast in some lower vertebrates—A comparative study of the ontogenetic development of the anterior mesoblast in *Petromyzon*, *Etmopterus*, *Torpedo*, et al. Lund: Hakan Ohlsson Boktryckeri; 1949.
11. Jarvik E. Basic structure and evolution of vertebrates, vol. 1. New York: Academic Press; 1980.
12. Adachi N, Kuratani S. Development of head and trunk mesoderm in the dogfish, *Scyliorhinus torazame*: I. embryology and morphology of the head cavities and related structures. *Evol Dev*. 2012;14(3):234–56.
13. Balfour FM. A monograph on the development of elasmobranch fishes. MacMillan; 1878.
14. Platt JB. A contribution to the morphology of the vertebrate head, based on a study of *Acanthias vulgaris*. *J Morphol*. 1891;5:79–106.
15. Neal HV. The history of the eye muscles. *J Morphol*. 1918;30:433–53.
16. Goodrich ES. On the development of the segments of the head in *Scyllium*. *Quart J micr Sci*. 1918;63:1–30.
17. van Wijhe JW. Über die Mesodermsegmente und die Entwicklung der Nerven des Selachierkopfes. *Verh Kon Akad Wetensch Amsterdam*. 1882;22:1–50.
18. Kuratani S, Ahlberg PE. Evolution of the vertebrate neurocranium: problems of the premandibular domain and the origin of the trabecula. *Zool Lett*. 2018;4(1):1.
19. Bertmar G. On the ontogeny of the chondral skull in Characidae, with a discussion on the chondrocranial base and the visceral chondrocranium in fishes. *Acta Zool*. 1959;40(2–3):203–364.
20. Jollie M. Segmentation of the vertebrate head. *Am Zool*. 1977;17:323–33.
21. Kuratani S, Horigome N, Hirano S. Developmental morphology of the head mesoderm and reevaluation of segmental theories of the vertebrate head: evidence from embryos of an agnathan vertebrate, *Lampetra japonica*. *Dev Biol*. 1999;210(2):381–400.
22. Adelman HB. The development of the eye muscles of the chick. *J Morphol Physiol*. 1927;44(1):29–87.
23. Tanaka S. Notes on some Japanese fishes, with descriptions of fourteen new species. *Journ Coll Sci Imp Univ Tokyo*. 1908;23:1–55.
24. Ballard WW, Mellinger J, Leichenault H. A series of normal stages for development of *Scyliorhinus canicula*, the lesser spotted dogfish (*Chondrichthyes: Scyliorhinidae*). *J Exp Zool*. 1993;267:318–36.
25. Hara Y, Yamaguchi K, Onimaru K, Kadota M, Koyanagi M, Keeley SD, Tatsumi K, Tanaka K, Motone F, Kageyama Y, Nozu R, Adachi N, Nishimura O, Nakagawa R, Tanegashima C, Kiyatake I, Matsumoto R, Murakumo K, Nishida K, Terakita A, Kuratani S, Sato K, Hyodo S, Kuraku S. Shark genomes provide

- insights into elasmobranch evolution and the origin of vertebrates. *Nat Ecol Evol.* 2018;2(11):1761–71.
26. Katoh K, Standley DM. MAFFT multiple sequence alignment software version 7: improvements in performance and usability. *Mol Biol Evol.* 2013;30(4):772–80.
 27. Sánchez R, Serra F, Tárraga J, Medina I, Carbonell J, Pulido L, de María A, Capella-Gutiérrez S, Huerta-Cepas J, Gabaldón T, Dopazo J, Dopazo H. Phylemon 2.0: a suite of web-tools for molecular evolution, phylogenetics, phylogenomics and hypotheses testing. *Nucleic Acids Res.* 2011;39(suppl_2):W470–4.
 28. Guindon S, Dufayard J-F, Lefort V, Anisimova M, Hordijk W, Gascuel O. New algorithms and methods to estimate maximum-likelihood phylogenies: assessing the performance of PhyML 3.0. *Syst Biol.* 2010;59(3):307–21.
 29. Minarik M, Stundl J, Fabian P, Jandzik D, Metscher BD, Psenicka M, Gela D, Osorio-Perez A, Arias-Rodriguez L, Horacek I, Cerny R. Pre-oral gut contributes to facial structures in non-teleost fishes. *Nature.* 2017;547(7662):209–12.
 30. Sugahara F, Murakami Y, Kuratani S. Gene expression analysis of lamprey embryos. In: Hauptmann G, editor. *In Situ Hybridization Methods*. New York: Springer New York; 2015. p. 263–78.
 31. Bevilacqua M. Guide to image editing and production of figures for scientific publications with an emphasis on taxonomy image editing for scientific publications. *Zoosystematics Evol.* 2020;96:139.
 32. Schweitzer R, Chyung JH, Murtaugh LC, Brent AE, Rosen V, Olson EN, Lassar A, Tabin CJ. Analysis of the tendon cell fate using Scleraxis, a specific marker for tendons and ligaments. *Development.* 2001;128(19):3855–66.
 33. Bonnin M-A, Laclef C, Blaise R, Eloy-Trinquet S, Relaix F, Maire P, Duprez D. *Six1* is not involved in limb tendon development, but is expressed in limb connective tissue under *Shh* regulation. *Mech Dev.* 2005;122(4):573–85.
 34. Chen JW, Galloway JL. The development of zebrafish tendon and ligament progenitors. *Development.* 2014;141(10):2035–45.
 35. De Beer GR. The development of the vertebrate skull. London: Oxford University press; 1937.
 36. Holmgren N. Studies on the head in fishes - embryological, morphological, and phylogenetical researches. Part: development of the skull in sharks and rays. *Acta Zool.* 1940;21:51–267.
 37. Marshall AM. On the head cavities and associated nerves of elasmobranchs. *Quart J micr Sci.* 1881;21:72–97.
 38. Dohrn A. Studien zur Urgeschichte des Wirbelthierkörpers. Mittheilungen aus der Zoologischen Station zu Neapel. 1904;17:1–294.
 39. De Beer GR. Memoirs: The prootic somites of heterodontus and of amia. *Quart J Micro Sci.* 1924;52–68(269):17–38.
 40. Brent AE, Schweitzer R, Tabin CJ. A somitic compartment of tendon progenitors. *Cell.* 2003;113:235–48.
 41. Dietrich S, Schubert FR, Healy C, Sharpe PT, Lumsden A. Specification of the hypaxial musculature. *Development.* 1998;125(12):2235–49.
 42. Nassari S, Duprez D, Fournier-Thibault C. Non-myogenic contribution to muscle development and homeostasis: the role of connective tissues. *Front Cell Dev Biol.* 2017;5:22.
 43. Couly GF, Coltey PM, Le Douarin NM. The triple origin of skull in higher vertebrates: a study in quail-chick chimeras. *Development.* 1993;117:409–29.
 44. Platt JB. Ectodermic origin of the cartilage of the head. *Anat Anz.* 1893;8:506–9.
 45. Noden DM. Interactions and fates of avian craniofacial mesenchyme. *Development.* 1988;103(Supplement):121–40.
 46. Borue X, Noden DM. Normal and aberrant craniofacial myogenesis by grafted trunk somitic and segmental plate mesoderm. *Development.* 2004;131(16):3967–80.
 47. Noden DM. Patterning of avian craniofacial muscles. *Dev Biol.* 1986;116:347–56.
 48. Grenier J, Teillet MA, Grifone R, Kelly RG, Duprez D. Relationship between neural crest cells and cranial mesoderm during head muscle development. *PLoS One.* 2009;4(2):e4381.
 49. Tokita M, Schneider RA. Developmental origins of species-specific muscle pattern. *Dev Biol.* 2009;331(2):311–25.
 50. Noden DM, Francis-West P. The differentiation and morphogenesis of craniofacial muscles. *Dev Dyn.* 2006;235(5):1194–218.
 51. Noden DM. The role of the neural crest in patterning of avian cranial skeletal, connective, and muscle tissues. *Dev Biol.* 1983;96(1):144–65.
 52. Wachtler F, Jacob M. Origin and development of the cranial skeletal muscles. *Bibl Anat.* 1986;29:24–46.
 53. Mootoosamy RC, Dietrich S. Distinct regulatory cascades for head and trunk myogenesis. *Development.* 2002;129(3):573–83.
 54. Sefton EM, Kardon G. Chapter Five - Connecting muscle development, birth defects, and evolution: an essential role for muscle connective tissue. In: Wellik DM, editor. *Current Topics in Developmental Biology*, vol. 132. United States: Academic Press; 2019. p. 137–76.
 55. Heude E, Bellessort B, Fontaine A, Hamazaki M, Treier A, Treier M, Levi G, Narboux-Nême N. Etiology of craniofacial malformations in mouse models of blepharophimosis, ptosis and epicanthus inversus syndrome. *Hum Mol Genet.* 2015;24(6):1670–81.
 56. McBratney-Owen B, Iseki S, Bamforth SD, Olsen BR, Morriss-Kay GM. Development and tissue origins of the mammalian cranial base. *Dev Biol.* 2008;322(1):121–32.
 57. Chawla B, Schley E, Williams AL, Bohnsack BL. Retinoic acid and *Pitx2* regulate early neural crest survival and migration in craniofacial and ocular development. *Birth Defects Res B Dev Reprod Toxicol.* 2016;107(3):126–35.
 58. Creuzet S, Vincent C, Couly G. Neural crest derivatives in ocular and periorcular structures. *Int J Dev Biol.* 2005;19(2–3):161–71.
 59. Heude E, Tesarova M, Sefton EM, Jullian E, Adachi N, Grimaldi A, Zikmund T, Kaiser J, Kardon G, Kelly RG, Tajbakhsh S. Unique morphogenetic signatures define mammalian neck muscles and associated connective tissues. *eLife.* 2018;7:e40179.
 60. Adachi N, Bilio M, Baldini A, Kelly RG. Cardiopharyngeal mesoderm origins of musculoskeletal and connective tissues in the mammalian pharynx. *Development.* 2020;147(3):dev185256.
 61. Sleight VA, Gillis JA. Embryonic origin and serial homology of gill arches and paired fins in the skate, *Leucoraja erinacea*. *eLife.* 2020;9:e60635.
 62. Matsuoka T, Ahlberg PE, Kessarar N, Iannarelli P, Dennehy U, Richardson WD, McMahon AP, Koentges G. Neural crest origins of the neck and shoulder. *Nature.* 2005;436(7049):347–55.
 63. Sefton EM, Piekarski N, Hanken J. Dual embryonic origin and patterning of the pharyngeal skeleton in the axolotl (*Ambystoma mexicanum*). *Evol Dev.* 2015;17(3):175–84.
 64. Teng CS, Cavin L, Maxson REJ, Sánchez-Villagra MR, Crump JG. Resolving homology in the face of shifting germ layer origins: lessons from a major skull vault boundary. *eLife.* 2019;8:e52814.

Publisher's Note

Springer Nature remains neutral with regard to jurisdictional claims in published maps and institutional affiliations.

Ready to submit your research? Choose BMC and benefit from:

- fast, convenient online submission
- thorough peer review by experienced researchers in your field
- rapid publication on acceptance
- support for research data, including large and complex data types
- gold Open Access which fosters wider collaboration and increased citations
- maximum visibility for your research: over 100M website views per year

At BMC, research is always in progress.

Learn more biomedcentral.com/submissions

